



## Full Text View

[Volume 29, Issue 11 \(November 1999\)](#)

### Journal of Physical Oceanography

Article: pp. 2802–2828 | [Abstract](#) | [PDF \(1.05M\)](#)

# Sensitivity of Ventilation Rates and Radiocarbon Uptake to Subgrid-Scale Mixing in Ocean Models

**Matthew H. England\***

*Centre for Environmental Modelling and Prediction, School of Mathematics, University of New South Wales, Australia*

**Stefan Rahmstorf**

*Potsdam Institute for Climate Impact Research, Potsdam, Germany*

(Manuscript received January 7, 1997, in final form November 13, 1998)

DOI: 10.1175/1520-0485(1999)029<2802:SOVRAR>2.0.CO;2

### ABSTRACT

The sensitivity of ventilation timescales and radiocarbon ( $^{14}\text{C}$ ) uptake to subgrid-scale mixing parameterization is studied in a global ocean model. Seven experiments are examined that are identical in every manner except their representation of subgrid-scale mixing of tracers. The cases include (i) two runs with traditional Cartesian mixing (HOR), (ii) a run with enhanced isopycnal mixing (ISO), and (iii) four runs in which the effects of eddies on the mean ocean flow are parameterized following Gent and McWilliams (GM). Horizontal, isopycnal, and isopycnal-thickness diffusion coefficients are varied sequentially in the model runs. Of particular interest is the role of the tracer mixing schemes in influencing longer timescale ventilation processes—centennial and beyond—such as deep water mass renewal and circulation.

Simulated ventilation timescales and  $^{14}\text{C}$  vary greatly between the three mixing schemes. The isopycnal mixing run exhibits the most rapid water mass renewal due to strong diffusion effects and excessive surface convective overturn, particularly in the Southern Ocean. In contrast, the GM cases show much more gradual renewal of deep and bottom waters, with limited vertical convection of surface waters and slower abyssal currents. Under GM, a background horizontal diffusion or altered isopycnal mixing do not significantly change interior ocean ventilation rates. This means modelers can adjust these background diffusion coefficients under GM (for numerical purposes) without significantly changing model ventilation rates. Reducing the GM isopycnal thickness diffusivity, on the other hand, noticeably increases simulated deep water ventilation rates. In comparison with the HOR runs, deep and bottom

#### Table of Contents:

- [Introduction](#)
- [Model description](#)
- [Model ocean circulation](#)
- [Simulated water mass](#)
- [Discussion and conclusions](#)
- [REFERENCES](#)
- [TABLES](#)
- [FIGURES](#)

#### Options:

- [Create Reference](#)
- [Email this Article](#)
- [Add to MyArchive](#)
- [Search AMS Glossary](#)

#### Search CrossRef for:

- [Articles Citing This Article](#)

#### Search Google Scholar for:

- [Matthew H. England](#)
- [Stefan Rahmstorf](#)

water ventilation timescales are reduced by about 30% in ISO, and increased

by 30%–40% under GM. Comparison is made between model simulated and observed  $^{14}\text{C}$ . The GM runs appear to be the least successful in the North Atlantic Ocean, exhibiting very gradual and only shallow water-mass renewal compared to observations. In the Pacific and Indian Oceans, the HOR and ISO runs are ventilated too rapidly due to strong convection and water-mass contribution from the Southern Ocean. In contrast, the GM runs simulate spuriously old and  $^{14}\text{C}$ -depleted bottom and middepth water. The GM cases do, however, capture realistic  $^{14}\text{C}$  in the upper 1500 m of the Indian and Pacific Oceans. Overall, none of the model cases reproduce global ocean ventilation rates over centennial timescales (under the chosen set of parameter values). Higher horizontal resolution and a spatially varying GM thickness diffusivity may be required before global models capture long timescale ocean renewal processes with some degree of fidelity.

## 1. Introduction

Global ocean general circulation models (GCMs) used in climate studies require a parameterization for the mixing effects of subgrid-scale eddies. This is because climate model resolution is typically several times coarser than the typical length scale of eddy variability in the ocean. There are three lateral mixing schemes commonly used in present-day ocean climate models: simple downgradient horizontal diffusion, enhanced along-isopycnal diffusion, and isopycnal thickness diffusion. These different mixing schemes appear to greatly affect the model simulation of global-scale circulation and water-mass formation.

Many studies have been made of the sensitivity of temperature–salinity in global ocean models to the choice of subsurface mixing scheme (e.g., [England 1993](#); [Hirst and Cai 1994](#); [Danabasoglu et al. 1994](#); [Hirst and McDougall 1996](#); [McDougall et al. 1996](#); [Duffy et al. 1997](#); [Guilyardi et al. 1999](#), manuscript submitted to *J. Phys. Oceanogr.*). Other studies have focused on the sensitivity of anthropogenic tracer uptake (e.g., [Duffy et al. 1995](#); [England 1995a](#); [Robitaille and Weaver 1995](#); [Dixon et al. 1996](#); [England and Hirst 1997, hereafter EH97](#); [England and Holloway 1998](#)), these tracers typically resolving the decadal timescale. However, the sensitivity of longer timescale (centennial to millennial) ocean ventilation to the choice of model mixing scheme remains largely unexplored. This study and that of [Duffy et al. \(1997\)](#) are the only known reports of the role of mixing in determining overall model ventilation rates as monitored by simulated radiocarbon ( $^{14}\text{C}$ ) and in our study, water-mass age.

The World Ocean circulation at its largest scale involves a gradual renewal or ventilation of the interior ocean by water that was once at the sea surface. The age of seawater is then defined as the time elapsed since a given water mass was last exposed to the atmosphere. Any water sample will have some characteristic age distribution depending on where its source waters have come from and how long they have taken in their journey from the sea surface. The timescale for deep water renewal appears to be of the order of centuries to several millennia (e.g., [Stuiver et al. 1983](#); [England 1995b, hereafter E95](#)). Information on the rate of ocean ventilation at such long timescales is normally derived from measurements of oceanic radiocarbon. This is because  $^{14}\text{C}$  is one of the only long-living radionuclides that is easy to measure in seawater (see review by [England and Maier-Reimer 1999](#)).

It is important that models be able to approximately reproduce the renewal processes and ventilation timescales operating in the global ocean. For example, the rate of surface water overturn and ventilation determines the ocean's role in moderating climate change. The response of a climate model to atmospheric change is determined, in part, by the way the ocean model redistributes heat vertically and meridionally, and therefore by the nature and timing of ocean ventilation. Another important example is the study of carbon uptake by the oceans, normally estimated using an ocean GCM including biogeochemical processes. The air–sea flux of carbon dioxide will be determined, in part, by the rapidity of surface water overturn in the ocean model and therefore on the timescales of ocean ventilation.

The present study is an extension of E95, wherein an assessment was made of water mass age in a global ocean model. The age tracer represents the volume-weighted mean time for surface waters to renew a given interior water mass. In this paper we extend the study of E95 to cover a more detailed analysis of the sensitivity of modeled water mass age to the choice of interior ocean mixing scheme. In addition,  $^{14}\text{C}$  is simulated in order to facilitate a direct model–observation comparison of ocean ventilation. Seven experiments are considered that are identical in every manner apart from their representation of internal lateral mixing. The cases cover (i) two runs with standard Cartesian mixing (HOR), (ii) a run with enhanced isopycnal mixing (ISO), and (iii) four runs in which the effects of eddies on the mean ocean flow are parameterized following [Gent and McWilliams \(1990, hereafter GM\)](#). The GM runs include a standard case without background horizontal diffusion, another in which horizontal diffusion is maintained, and a third wherein the isopycnal tracer diffusion is altered. In the final GM case, the isopycnal thickness diffusivity is halved.

The two main goals of this study are as follows: First, to demonstrate that different model mixing schemes and

diffusivities drive substantially different rates of interior ocean ventilation and water mass renewal in the deep ocean. These model differences will be explained in terms of changes in ocean currents, convective overturn, and mixing brought about by altering the lateral diffusion scheme. Second, we hope to ascertain whether any of the ocean mixing schemes used can give a faithful representation of deep-water overturning timescales in the global ocean. This will be determined largely by comparing modeled and observed radiocarbon in the deep ocean.

The rest of this paper is divided into four sections. We describe the ocean model, experimental design, age tracer, and  $^{14}\text{C}$  simulations in [section 2](#). The general circulation of the model cases is summarized in [section 3](#), with particular focus on the vertical convection, meridional overturning, and the effects of mixing. In [section 4](#) we discuss the simulations of age and  $^{14}\text{C}$  in the seven model experiments. Finally [section 5](#) covers the discussion and conclusions.

## 2. Model description

### a. The ocean model

The ocean model used is the MOM version of the Bryan–Cox ocean GCM developed at the Geophysical Fluid Dynamics Laboratory ([Bryan 1969](#); [Cox 1984](#); [Pacanowski et al. 1991](#)). The model has a global coverage of the World Ocean with a realistic representation of ocean bottom bathymetry and continental outlines. The model grid spacing is  $4.5^\circ$  latitude by  $3.75^\circ$  longitude with 21 unequally spaced vertical levels. The specific configuration of the model runs is similar to that used in the CFC uptake study of EH97, except that all model cases have 21 vertical levels.

The background viscosity and vertical diffusion coefficients are identical in all model cases. Vertical mixing of tracers can be enhanced along isopycnal surfaces (ISO and GM cases) and when gravitational instability is detected. Convection is thereby treated implicitly in the model; whenever instabilities in stratification are detected, the vertical diffusion rate is increased to simulate complete mixing over the unstable portions of the water column. As such, the model parameterization of convection does not strictly involve a circulation; tracers are mixed vertically outside any calculation of vertical motion. Generally, downward motion will be induced in a region of strong convection, though certain instances of vertical convection can actually induce an upward motion in the velocity field ([Rahmstorf 1995](#)).

The model is forced by seasonally varying climatological boundary conditions of temperature, salinity, and wind stress. Temperature ( $T$ ) and salinity ( $S$ ) are damped toward the climatological values of [Levitus \(1982\)](#) with uniform restoring timescales of 30 days for  $T$  and 50 days for  $S$ . The wind stress climatology used is that of [Hellerman and Rosenstein \(1983\)](#). In all experiments considered, the ocean model is integrated with a synchronous  $T/S$  time step of one day at all depths and integrated until an annual cycle equilibrium is achieved in simulated  $T$ ,  $S$ ,  $^{14}\text{C}$ , and age. We use the following criteria: annual mean changes of less than  $0.005^\circ\text{C}$  ( $T$ ),  $0.001$  psu ( $S$ ),  $0.1\text{‰}$  ( $^{14}\text{C}$ ), and 0.5 years (age) per century of integration are required over all model grid points. The integration times required in the respective model cases are included in [Table 1](#).

### b. Experimental design

Each case is identical in every manner apart from the treatment of lateral/isopycnal mixing ([Table 1](#)). The first experiment (HOR-Z) adopts traditional Cartesian mixing with a depth-dependent horizontal diffusivity  $A_{\text{HH}}$  ( $1.0 \times 10^3 \text{ m}^2 \text{ s}^{-1}$  in the surface level decreasing toward  $0.5 \times 10^3 \text{ m}^2 \text{ s}^{-1}$  at depth; as in [Bryan and Lewis 1979](#)). A second HOR case (HOR = 0.75) adopts a constant horizontal diffusivity  $A_{\text{HH}} = 0.75 \times 10^3 \text{ m}^2 \text{ s}^{-1}$  to facilitate direct comparison with ISO. The isopycnal mixing experiment (ISO) features the introduction of the widely used scheme of [Cox \(1987\)](#) that includes the effect of tracer diffusion along isopycnal surfaces. Under this scheme, the horizontal diffusivity must be maintained for numerical stability; in ISO it takes the constant value of  $A_{\text{HH}} = 0.75 \times 10^3 \text{ m}^2 \text{ s}^{-1}$ . The isopycnal diffusion decreases gradually between the surface and bottom levels ( $5.0 \times 10^3 \text{ m}^2 \text{ s}^{-1}$  in the surface layer decreasing to  $1.0 \times 10^3 \text{ m}^2 \text{ s}^{-1}$  at depth); as such, the choice of isopycnal and horizontal diffusivity in ISO is exactly as in [Manabe et al. \(1991\)](#).


The other four experiments feature the scheme of GM and [Gent et al. \(1995\)](#) for representing adiabatic transport effects of baroclinic eddies. The implementation of the Gent et al. parameterization is as detailed in [Hirst and McDougall \(1996\)](#) and EH97. As in EH97 and many other studies, the isopycnal thickness diffusivity ( $\kappa$ )—which determines the strength of the eddy-induced tracer transports—is set to  $1.0 \times 10^3 \text{ m}^2 \text{ s}^{-1}$  in all GM cases except GM = 0.5. The GM runs also carry the isopycnal tracer diffusion as used in ISO. In the first GM experiment (GM-0), the background horizontal diffusivity is set to zero and the depth-dependent profile  $A_\rho(z)$  of ISO is maintained. In the second case (GM-H), we retain the background horizontal diffusivity used in ISO ( $A_{\text{HH}} = 0.75 \times 10^3 \text{ m}^2 \text{ s}^{-1}$ ). In GM = ISO, the isopycnal ( $A_\rho$ ) and isopycnal thickness ( $\kappa$ ) diffusion coefficients are set to the same value following the recommendations of [Dukowicz and Smith \(1997\)](#). Zero

horizontal diffusivity is maintained and  $A_\rho = \kappa = 1.0 \times 10^3 \text{ m}^2 \text{ s}^{-1}$ . Finally, in GM = 0.5, we rerun GM-0 with a reduced isopycnal thickness diffusivity of  $\kappa = 0.5 \times 10^3 \text{ m}^2 \text{ s}^{-1}$ . When discussing the GM runs, experiment GM-0 will be considered the “control” GM case.

In our experimental design, we only consider spatially and temporally constant values of  $\kappa$ . A value of  $\kappa = 1 \times 10^3 \text{ m}^2 \text{ s}^{-1}$  is supported by the analysis of [Rix and Willebrand \(1996\)](#) of an eddy-resolving Atlantic model with  $\frac{1}{3}^\circ$  horizontal resolution. They perform their analysis of the GM thickness diffusion term for a region of the North Atlantic ( $10^\circ\text{--}30^\circ\text{N}$ ,  $20^\circ\text{--}60^\circ\text{W}$ ). On the other hand, [Visbeck et al. \(1997\)](#) present strong arguments that the value of  $\kappa$  should depend on the local vertical and horizontal stratification, and varies by an order of magnitude or so between different regions of the ocean. They use idealized experiments to estimate that  $\kappa$  should be  $2.0 \times 10^3 \text{ m}^2 \text{ s}^{-1}$  in a wind-driven channel resembling the Antarctic Circumpolar Current, but only  $0.3 \times 10^3 \text{ m}^2 \text{ s}^{-1}$  in a typical convection region. It is recommended that a future study be carried out simulating water mass age and radiocarbon with a spatially varying parameterization of  $\kappa$ .

### *c. The age tracer*

Following [Thiele and Sarmiento \(1990\)](#) and E95, the model ocean age of water ( $A$ ) is defined according to the equation  $dA/dt = L(A) + 1$ , where  $L(A)$  refers to the standard tracer diffusion and convection terms in the model, and  $t$  is time. In addition,  $A$  obeys the boundary condition  $A(x, y, z) = 0$  at the uppermost model level, and the initial condition  $A(x, y, z) = 0$  over the global domain. In effect,  $A$  is incremented by the model time step during each time step, with the only processes limiting the indefinite growth of  $A$  associated with the ventilation of the ocean interior by water originating from the sea surface. By definition, water in direct contact with the sea surface (i.e., the upper model level) retains an age of zero throughout the model integration. Regions of persistent surface convective overturn acquire near-zero age during wintertime months, whereas remote deep waters accumulate age values that asymptotically approach their true age as all source waters gradually ventilate the region.

The age tracer is of little value until the entire age field is completely equilibrated. To ensure that  $A$  represents the true age of the model water masses, the age experiments are run until little change in age is detected throughout the model domain (a criterion of less than 6 months aging per 100 years integration is required over all model grid points; see also [Table 1](#) ) .

### *d. Radiocarbon simulations*

Pre-industrial radiocarbon is simulated in the ocean model using the technique described by [Toggweiler et al. \(1989\)](#). Only pre-industrial radiocarbon is considered: we do not simulate the oceanic uptake of bomb-produced  $^{14}\text{C}$ . The model calculates the deviation of the oceanic  $^{14}\text{C}/^{12}\text{C}$  ratio from a standard atmospheric ratio, this deviation is given the notation  $\Delta^{14}\text{C}$ . The pre-industrial atmospheric  $^{14}\text{C}/^{12}\text{C}$  reference ratio is taken to be zero. Thus defined, prebomb oceanic  $\Delta^{14}\text{C}$  is normally negative since the  $^{14}\text{C}$  isotope decays in the ocean. The more negative the value of  $\Delta^{14}\text{C}$ , the more time has elapsed since the water mass was last in contact with the atmosphere.

Because the  $\Delta^{14}\text{C}$  ratio is the quantity simulated in the model, not the absolute concentration of  $^{14}\text{C}$ , biological conversion processes can be largely ignored because they affect  $^{12}\text{C}$  and  $^{14}\text{C}$  compounds in the same manner ([Fiadiero 1982](#)). In addition, because  $\Delta^{14}\text{C}$  simulations do not predict gas transfer on the basis of actual  $^{12}\text{CO}_2$  and  $^{14}\text{CO}_2$  concentration levels, isotopic fractionation between gaseous and dissolved  $\text{CO}_2$  phases can be neglected. This means that the prebomb cycle of  $\Delta^{14}\text{C}$  can be forced toward a time-independent atmospheric value of zero. The gas exchange rate is taken to be wind speed dependent in the open ocean and zero in regions and times of observed sea-ice coverage. The air–sea  $\Delta^{14}\text{C}$  flux is also calibrated to match observed global mean gas exchange rates (as in experiment P' of [Toggweiler et al. 1989](#)). Interior  $\Delta^{14}\text{C}$  then gets redistributed by the model circulation, convection, and mixing processes (exactly as for  $T\text{--}S$ ), as well as undergoing natural radioactive decay with a  $^{14}\text{C}$  half-life of 5730 years.

## **3. Model ocean circulation, vertical convection, and mixing**

### *a. Vertical convection*

The location and timescale of ocean ventilation is determined by convection, mixing, and vertical velocity in regions of water mass formation and in addition by the horizontal circulation and lateral diffusion in regions not directly ventilated by water at the sea surface. Near regions of deep-water formation the convective activity of the model is somewhat more



important than the meridional overturning (see also [Karoly et al. 1997](#)). This is because the model's timescale for convective adjustment (hours to days) is much more rapid than the timescale for vertical motion ([England et al. 1994](#)). The maximum penetration depth of surface water convection is shown for three model cases in [Fig. 1](#) (HOR-Z, GM-0, and GM = 0.5). The maps represent the maximum convection depth during an annual cycle of the equilibrated ocean states. Convection patterns in each HOR run and the ISO experiment are largely the same (EH97), so only HOR-Z is shown. Likewise, convective layer depths in GM-0, GM-H, and GM = ISO are almost identical, so we only include a plot of GM-0. For comparison with observations, the depth of the wintertime mixed layer is included in [Fig. 1a](#). Convection is intense during the wintertime months and nearly absent during summer because of the stabilization of the surface mixed layer by summer heating (see also EH97). Included in the analysis for the ISO and GM cases are those regions where the slope of the isopycnal surfaces exceeds 1 part in 100 (corresponding to the maximum slope set for isopycnal diffusion), which generates vertical diffusion terms that partly mimic and replace explicit convective mixing ([Hirst and Cai 1994; EH97](#)). It should also be noted that isolated subsurface convection can occur underneath stably stratified surface layers. This is not shown in the diagnostic of [Fig. 1](#), partly because it is difficult to depict, but also because our interest here is on direct ventilation of surface waters into the ocean interior.

The HOR and ISO cases both show extensive deep convection in the Southern Ocean. This is due to unrealistically weak stratification in the upper 1500 m of the water column at 55° to 70°S, a consequence of insufficient density of the model-equivalent of Circumpolar Deep Water (CDW: see [Fig. 2](#)). This widespread deep convection conflicts with observations, which show upwelling of old CDW and shallow surface mixed layers at these latitudes ([Fig. 1a](#)). For example, oxygen-depleted CDW is seen to upwell toward the surface 500 m at 55°–70°S ([Fig. 3](#)), leaving intense vertical gradients in oxygen content that are suggestive of very stable upper-ocean stratification. Oxygen-enriched surface water ventilation of the interior is only noted south of 70°S and north of the Polar Frontal Zone (PFZ) near 55°S. Even during winter, surface mixed layers are typically only 50–100 m thick at these latitudes ([Fig. 1a](#)). This contrasts the very deep mixed layers simulated in HOR and ISO ([Figs. 1b, 2b](#)). Unlike the HOR and ISO cases, convection in all GM experiments is largely limited to the Antarctic shelf and north of the PFZ, both thought to be regions of convective mixed layer formation (e.g., [McCartney 1977; Killworth 1983](#); see also [Fig. 1a](#)). This is because CDW is much denser under GM, leaving the Southern Ocean more realistically stratified ([Fig. 2c](#)).

The pattern of convection in the North Atlantic varies less between the model runs than that in the Southern Ocean. The HOR and ISO cases yield similar patterns. Convective overturn is moderately weaker in the GM cases, with somewhat shallower penetration of convective instability and a general reduction in the extent of the convection area. For example, in GM-0 deep convection in the North Atlantic contracts to two isolated grid points: one off southeast Greenland and the other farther north in the Norwegian Basin, with maximum convection depths of order 700–1000 m. Within the GM experiments, more convective overturn is noted when the isopycnal thickness diffusivity ( $\kappa$ ) is decreased (GM = 0.5). This is related to reduced stratification when  $\kappa$  is weakened. Including horizontal diffusion (GM-H) or reducing the isopycnal diffusivity (GM = ISO), on the other hand, does not significantly alter the convection patterns seen in GM-0.

## *b. Vertical advection*

Surface layer vertical motion is largely determined by the surface Ekman transport and therefore the surface wind stress, so little variation is noted between the model experiments. As an overview, [Fig. 4](#) shows the vertical velocity at the base of the surface layer in the HOR-Z, ISO, and GM-0 runs. Included in the GM-0 panel is the additional eddy-induced vertical velocity  $w^*$  due to the divergence in the horizontal GM eddy advection field. The large-scale Eulerian vertical velocity distribution is nearly identical in all experiments. Only the effects of  $w^*$  distinguish the vertical velocity field in the GM experiments from that in the other runs. All the small-scale regional upwelling and downwelling features apparent in the HOR and ISO experiments are representative of the Eulerian velocity component in the GM runs. Differences seen in [Fig. 4c](#) are almost entirely due to  $w^*$ ; for example, the region of strong downward advection in the Greenland Sea is associated with a convergence in the eddy-induced horizontal advection field in that region.

In all experiments thermocline water is upwelled strongly in the near-equatorial oceans. Farther south, CDW is upwelled nearly uniformly under the subpolar westerlies (apart from some small-scale downward advection regions associated with  $w^*$  in the GM runs). This means that in the HOR and ISO runs, paradoxically, much of the surface layer convection in the Southern Ocean ([Fig. 1b](#)) takes place in a region of broad wind-driven upwelling. This is not the case under GM, wherein convection is largely absent under the subpolar westerly wind belt ([Fig. 1](#)).

In regions of surface downwelling (largely in the subtropical convergence zone), direct ventilation of the thermocline occurs via the vertical advective fields. This crudely corresponds to the model equivalent of the ventilated thermocline of [Luyten et al. \(1983\)](#). In regions of near-surface upwelling, older water is entrained into the upper model levels, yielding a mixture of thermocline water that is older than that directly ventilated by the wind-driven circulation.

## *c. Meridional overturning*

The global and Atlantic meridional overturning streamfunctions for the HOR-Z, GM-0, and GM = 0.5 cases are included in [Fig. 5](#). The meridional overturning in the other experiments is not shown since ISO and HOR = 0.75 are very similar to HOR-Z, and the GM-H and GM = ISO runs are largely similar to GM-0. The effective transport velocity (i.e., resolved Eulerian velocity plus eddy-induced transport velocity) is used to calculate the overturning streamfunction for the GM cases since this quantity is the most relevant to the redistribution of tracers in the model.

Despite increased vertical resolution, HOR-Z and ISO display similar overturning to the equivalent model cases described in EH97. As in that study, the ISO and HOR-Z runs have very similar meridional overturning because the isopycnal diffusion terms largely mix tracers without generating different overturning rates. All three GM cases with  $\kappa = 1.0 \times 10^3 \text{ m}^2 \text{ s}^{-1}$  exhibit nearly identical overturning streamfunctions, demonstrating that the horizontal and isopycnal diffusion terms are weak in GM-H and GM = ISO, respectively. In GM-H, this is because isopycnal surfaces are flatter under GM, thereby reducing the spurious diapycnal diffusion normally caused by  $A_{\text{HH}}$ . Contrasting GM-H and GM = ISO, halving  $\kappa$  in GM = 0.5 noticeably increases the meridional overturning. This is particularly so in the North Atlantic ([Fig. 5f](#)), with a notably more vigorous overturning of NADW in GM = 0.5 (up from 12.9 to 16.2 Sv:  $\text{Sv} \equiv 10^6 \text{ m}^3 \text{ s}^{-1}$ ).

In HOR-Z, the production rate of North Atlantic Deep Water (NADW) is realistic at 20.6 Sv, although only 8.7 Sv flows out into the Southern Ocean. Similar transport values are noted in ISO (19.0 Sv NADW production; 7.8 Sv outflow), whereas the GM cases with high  $\kappa$  exhibit a marked shoaling of NADW outflow (depth 1000–1800 m compared to 1500–2300 m in HOR-Z) and generally weaker production and outflow rates (approximately 13 Sv NADW production and 7 Sv outflow in the GM-0, GM-H, and GM = ISO cases). Though a little stronger, NADW overturn and outflow is also too weak in GM = 0.5. This weakening of NADW flow could indicate that the thickness diffusion coefficients used in our study are too strong for the North Atlantic convection regions, as discussed above and argued by [Visbeck et al. \(1997\)](#). A high value of the parameter  $\kappa$  tends to inhibit convection and deep-water formation by flattening isopycnal surfaces and increasing vertical stratification.

A total of 29.8 Sv of Antarctic Bottom Water (AABW) is overturned off Antarctica in HOR-Z, the majority upwelling south of 60°S. Again, similar transport values are noted in ISO and HOR = 0.75. In contrast, the direct Antarctic cell is dramatically weakened in the GM cases (about 7 Sv AABW production in all cases) and now appears as an extension of the deep cell. This change in AABW overturn is associated with changes in deep Antarctic densities under GM. After inclusion of the eddy-induced advection terms in the calculation of meridional overturn, the Deacon cell becomes very weak in the GM runs whether or not horizontal diffusion is present. This is because the indirect cell of the resolved Eulerian transport is partly cancelled by a direct cell resulting from the eddy-induced transport (as in [Danabasoglu et al. 1994](#); [Hirst and McDougall 1996](#); EH97). It should also be noted, however, that the Deacon cell in the HOR and ISO cases largely disappears when calculated as a transport streamfunction integrated in density–latitude coordinates (e.g., [Döös and Webb 1994](#); [Hirst et al. 1996](#)) and as such does not directly contribute to significant diapycnal tracer fluxes.

#### d. Mixing

The similarity in vertical convection and meridional overturn between the HOR and ISO cases suggests these runs should exhibit largely similar age and  $^{14}\text{C}$  distributions. However, it should be noted that the ISO case carries additional along-isopycnal diffusion that will act to reduce interior water age and increase  $^{14}\text{C}$ . With a typical upper-ocean isopycnal diffusivity of  $A_\rho = 4.0 \times 10^3 \text{ m}^2 \text{ s}^{-1}$ , we expect the isopycnal mixing terms to act over  $((A_\rho t)^{1/2}) \approx 1100 \text{ km}$  (in an along-isopycnal sense) during a timescale of  $t = 10 \text{ yr}$ . This will therefore be a process that influences rates of interior ocean ventilation in the ISO run, particularly in regions of steeply sloping isopycnal surfaces (e.g., the Southern Ocean, [Fig. 2b](#)).

Differences in horizontal, isopycnal, and isopycnal thickness diffusion coefficients in the GM runs will result in both *direct* and *indirect* differences in ocean ventilation rates. By direct effects we refer to changes in ventilation that relate simply to that mixing term in the tracer balance, whereas indirect effects are those that relate to the mixing altering the oceanic circulation and/or convection in some way. The direct effects are simple to predict for horizontal/isopycnal diffusion: stronger mixing coefficients should result in a slightly enhanced ventilation of interior waters. On the other hand, their indirect effects are quite weak under GM; namely, convection and meridional overturn are largely unchanged when horizontal/isopycnal diffusion rates are altered. For the GM thickness diffusion rate ( $\kappa$ ), in contrast, we noted a sensitivity of simulated convection and NADW overturn when comparing GM-0 and GM = 0.5. In particular, decreasing  $\kappa$  results in increased NADW overturn and slightly more widespread convective instability over the North Atlantic and Southern Oceans.

## 4. Simulated water mass age and radiocarbon

The simulated age of water in the World Ocean model experiments is summarized in [Table 2](#), which shows the oldest water mass mixtures obtained in several key regions of the ocean, including thermocline and deep waters. For comparison

with similar figures presented in E95, [Figs. 6–8](#) show the basin-averaged age in the Atlantic, Indian, and Pacific Oceans in runs HOR-Z, ISO, GM = 0.5, and GM = ISO. The GM = 0.5 and GM = ISO cases were selected as they represent the GM runs with the youngest and oldest deep waters, respectively (refer also to [Table 2](#)). The other GM runs (GM-0 and GM-H) are closest to GM = ISO in terms of their simulated age and  $\Delta^{14}\text{C}$ . To enable further intercomparison between model runs, [Fig. 9](#) shows the basinwide mean profiles of age in the North Atlantic, North Indian, North Pacific, and Southern Oceans in all experiments. A similar diagram is shown for radiocarbon; namely, basinwide mean profiles of  $\Delta^{14}\text{C}$  in the same model subregions ([Fig. 10](#)). In this diagram, observations of radiocarbon from the Geochemical Ocean Sections Study (GEOSECS) are also included for comparison. Bottom-water ventilation ages are given in [Table 3](#). Radiocarbon simulations are summarized in [Fig. 10](#) and [Table 4](#), the latter showing the mean model/observed  $\Delta^{14}\text{C}$  in key regions of the global ocean. Throughout this paper, age values are normally quoted to the nearest ten years and radiocarbon to the nearest part per thousand (ppt).

Broadly speaking, ventilation timescales are most rapid in ISO and slowest in the GM experiments with isopycnal thickness diffusion  $\kappa = 1.0 \times 10^3 \text{ m}^2 \text{ s}^{-1}$ . This is a result of the combined ventilation effects of vertical convection, meridional overturn, interior ocean currents, and mixing. Detailed regional tracer budget analyses have been performed for each experiment but are not included here. From such analyses it is confirmed that in the tracer term balance for age and  $\Delta^{14}\text{C}$ , convection is strongest in the HOR and ISO cases and weak under GM. Meridional overturning strength is also markedly reduced under GM compared with HOR and ISO. Interior lateral mixing affects age and  $\Delta^{14}\text{C}$  most in ISO and least under GM, even though GM-H carries all the mixing terms of ISO on top of the GM isopycnal thickness diffusion terms. This is because the ISO run simulates spuriously steep isopycnal surfaces in the circumpolar ocean ([Fig. 2](#)), whereas GM-H has quite realistically sloped density surfaces in the region (similar to GM-0 in [Fig. 2](#)). This is due to the isopycnal thickness diffusion term of GM, which acts to flatten isopycnal surfaces ([Gent et al. 1995](#)), leading to an overall reduction in the diapycnal mixing caused by  $A_{\text{HH}}$ . Finally, the flatter isopycnal surfaces under GM result in a reduction in interior geostrophic currents, which partly explains the reduced overturning rates in these runs.

These combined effects of convection, meridional overturn, interior currents, and mixing completely determine the ventilation timescales of the model runs; the oldest water mass mixture (located at middepth in the Pacific Ocean, i.e., NPDW) is dated at 1340 yr in HOR-Z, only 1010 yr in ISO, 1950 yr in GM-0, 1720 yr in GM = 0.5, and as much as 2010 yr in GM = ISO ([Table 2](#)). This trend in age between the model cases can be seen in many of the major water masses of the global ocean (see, e.g., [Fig. 9](#) and [Tables 2, 3](#)); namely, the order of ventilation rapidity across experiments is ISO (most rapid ocean ventilation), the HOR runs, GM = 0.5, GM-H, GM-0, then GM = ISO (most gradual ventilation). This is also apparent in intercomparisons of model simulated  $\Delta^{14}\text{C}$  (e.g., [Fig. 10](#) and [Table 4](#)).

Compared with the equivalent 12-level cases in E95, both HOR-Z and ISO have NPDW that is approximately 10% younger when run at a vertical resolution of 21 levels. The reason for this subtle increase in NPDW renewal rates is a slightly stronger overturning in the deep Antarctic cell when higher vertical resolution is adopted. This is due to the elimination of two gridpoint computational modes that can be excited at 12-level vertical resolution, and whose rotation sense counters the primary cell near the equator (as also noted by [Weaver and Sarachik 1990](#)).

In the following subsections we examine in more detail the regional distributions of age and  $\Delta^{14}\text{C}$  in the North Atlantic, Southern, North Pacific, and Indian Oceans. The age and  $\Delta^{14}\text{C}$  depth profiles provide the most concise means of intercomparing the respective model runs. With regards to the comparison with observed radiocarbon, it should be noted that upper ocean GEOSECS  $\Delta^{14}\text{C}$  measurements (made during 1972, 1974, and 1978) are contaminated by bomb-produced radiocarbon from nuclear testing in the 1950s and 1960s, whereas we only simulate natural  $^{14}\text{C}$ . However, away from bottom and intermediate water formation regions, the Pacific, Indian, and Southern Ocean bomb  $^{14}\text{C}$  contamination is negligible, and direct model–observed comparisons can be made. In the North Atlantic, some bomb  $^{14}\text{C}$  penetrates to 3000 m in regions of NADW formation, though much of the observed radiocarbon below 1000 m and south of  $40^\circ\text{N}$  is free of bomb contamination.

### *a. North Atlantic Ocean ventilation*

The age of NADW in the GM runs is markedly older than that in the ISO and HOR cases, even exceeding 1000 yr in the North Atlantic below 3000 m in the runs with  $\kappa = 1.0 \times 10^3 \text{ m}^2 \text{ s}^{-1}$ . In the real ocean, water in this region is ventilated by Lower NADW formed in the Greenland–Norwegian Seas; whereas in the model it is almost entirely of Southern Ocean origin (see [Fig. 5](#)). This old deep water in the North Atlantic is reflected in overly depleted  $^{14}\text{C}$  concentrations in the model experiments. [Figure 11](#) shows the observed western Atlantic GEOSECS section of  $^{14}\text{C}$  compared with model runs HOR-Z, ISO, and GM-0 (all GM cases are largely similar to GM-0, although GM = 0.5 exhibits slightly more  $^{14}\text{C}$

content at depth). Compared with observed  $^{14}\text{C}$ , all model experiments underestimate the depth of NADW penetration, with a clear delineation between upper well-ventilated NADW and lower  $^{14}\text{C}$ -depleted waters (particularly under GM). The observations suggest that the North Atlantic Ocean is relatively well ventilated at all depths (Fig. 11a). It seems that our model chronically underestimates the depth and vigor of NADW overturn, particularly under GM. Additional GM experiments with an enhanced seasonal cycle of  $T-S$  and/or inclusion of the topographic stress parameterization of Holloway (1992) did not rectify this problem.<sup>1</sup>

Bottom water in the far North Atlantic is as old as 1230 yr in GM = ISO, compared to 460 yr in HOR-Z and 420 yr in ISO (Table 3). None of the model cases simulate young Lower NADW (2500–4000-m depth; Fig. 9a); instead, water below 3000 m is ventilated from the Southern Ocean, with no direct renewal by deep water formed in the Norwegian–Greenland Sea. This is in contrast to the observed distribution of  $^{14}\text{C}$ , which suggests direct NADW ventilation to at least 4000-m depth north of the equator (Fig. 11a). This model problem was at first thought to be due to the smoothing of deep sills in the topography along the Greenland–Scotland Ridge, particularly in the GM cases. However, experimental runs with a deepened ridge system in the far North Atlantic showed negligible change in the depth of NADW overturn. It remains to be seen why GM causes such a shoaling of NADW outflow in our model domain.

Figure 12 shows a horizontal section of age in experiments HOR-Z, ISO, GM = ISO, and GM = 0.5 on the level of most rapid NADW outflow. Among the GM runs, GM = 0.5 and GM = ISO are shown as they simulate the youngest and oldest NADW under GM, respectively. Depth levels are chosen to coincide with the strongest outflow in the western boundary—the GM runs having a distinctly shallower thermohaline circulation in the Atlantic Ocean. The outflowing NADW progressively ages as it leaves the Atlantic basin. A signal of younger water is seen in the deep western boundary current outflow in each model case; however in ISO a substantial contamination of the outflowing NADW is made by Southern Ocean water, which is mixed and diffused northward in an extension of Antarctic Intermediate Water. Recent CFC simulations by England (1995a) and EH97 suggest that this feature of the ISO case is spurious and that less downward and northward spreading of waters should take place at this depth. NADW leaving the Atlantic sector is about 300 yr old in HOR-Z and less than 200 yr in ISO, compared with 400 yr in GM-0 and GM-H, and more than 500 yr in GM = ISO. The questionable Southern Ocean contamination of the deep South Atlantic in ISO is the main reason for young outflowing NADW in that model run.

### b. Southern Ocean ventilation

Figures 6–8 display the basin-averaged age in the Atlantic, Indian, and Pacific Oceans in HOR-Z, ISO, GM = 0.5, and GM = ISO. Runs GM-0 and GM-H have a similar though slightly younger age distribution to GM = ISO, so they are not included here. In each basin there is a clear signal of older CDW upwelling toward the surface near 60°S in the GM experiments. This is a distinct success of the GM parameterization over the standard Cartesian and isopycnal mixing schemes, and has been shown to correspondingly improve CFC simulations by England (1995a), Robitaille and Weaver (1995), and EH97. Both the HOR-Z and ISO cases have virtually no older water mass signal in CDW. For example, the Pacific Ocean variety of CDW at 1500-m depth is only 100 years old near 60°S in both HOR-Z and ISO, whereas it is almost 1000 years old in the GM runs. While the GM experiments have a clear stratification of age in the near-surface subpolar Southern Ocean, virtually no vertical age gradients can be seen in ISO and HOR-Z. The observed zonal mean section of oxygen concentration in the Southern Ocean (Fig. 3) suggests substantial vertical age gradients in the surface 1000 m near 55°–70°S, so the GM ventilation scheme for CDW is likely to be the most realistic of the model cases considered.

The mean profile of age simulated in the Southern Ocean is shown for each experiment in Fig. 9d. The latitude band selected is 55°–70°S, corresponding in the real ocean with the location of CDW upwelling and relatively stable surface layer stratification. The corresponding model simulations of radiocarbon at this latitude band are presented in Fig. 13, shown as a mean profile with standard deviation bars indicating the spread of  $^{14}\text{C}$  simulated at each depth level. GM-0 and GM-H are largely similar to GM = ISO, and so are not shown here. The overlaying scatterplot of GEOSECS  $^{14}\text{C}$  measurements facilitates a direct comparison between modeled and observed ventilation rates. From the model–observed comparison of  $^{14}\text{C}$ , it is clear that the model equivalent of CDW is too young in the HOR and ISO cases. The GEOSECS measurements of radiocarbon indicate a near-uniform Southern Ocean value of  $\Delta^{14}\text{C} = -160\text{‰}$  below 1000 m, whereas the HOR and ISO cases simulate radiocarbon to be depleted to only about  $-120\text{‰}$ . This is due to rapid and deep overturn of  $^{14}\text{C}$ -rich surface waters at this latitude band. In contrast, all GM cases do a reasonable job at capturing the upper 1000-m radiocarbon structure, but they overestimate the  $\Delta^{14}\text{C}$  depletion of CDW, indicating that this water mass is erroneously old under GM. This is particularly the case in the runs with  $\kappa = 1.0 \times 10^3 \text{ m}^2 \text{ s}^{-1}$ , where deep Southern Ocean  $\Delta^{14}\text{C}$  values approach  $-220\text{‰}$ .

Age profiles simulated in the Southern Ocean are dramatically different between the non-GM and GM runs (Fig. 9d).



In ISO, CDW has a typical age of only 150 yr. In the real ocean, outflowing NADW contributes a substantial component of the deep water in the Southern Ocean. In ISO, NADW attains an age of 200–300 yr as it flows into the Southern Ocean (Fig. 12b), and yet much of the CDW in this experiment is only 100–200 years old. This is due to the spurious deep convection that takes place at 55°–70°S in ISO. A similar inconsistency can be seen in the HOR runs; wherein NADW outflow (300–350 yr) is older than most of the model CDW (100–300 yr). In contrast to HOR-Z and ISO, upper NADW in the GM runs is somewhat younger (at 350–500 yr) than a substantial component of the model CDW (400–1000 yr). Clearly, the GM cases reduce the Southern Ocean's dominance of deep-water renewal that can be seen under HOR and ISO.

Relatively young deep waters can be found in each model run in the Weddell and Ross Seas (Figs. 12, 15; though Ross Sea Bottom Water is quite old under GM). In ISO, the young water signal is quite diffuse near these bottom-water formation zones, indicating rapid horizontal and isopycnal blending of the surface water signal as it is convected over the continental shelf. The HOR-Z case has moderate gradients in age near the bottom-water formation zones, while each GM run has a distinct concentration of younger water in only a few model grid points adjacent to Antarctica. This has been cited as one of the successes of the GM parameterization; it permits relatively confined downslope flows without spurious diapycnal dilution (e.g., Hirst and McDougall 1996). However, the timescale for downslope flow of AABW is somewhat too slow under GM, with bottom-water mixtures being spuriously old just off the Antarctic continent. This is demonstrated in Fig. 14, which compares the minimum age of AABW in the Weddell Sea in ISO and two of the GM runs (GM = 0.5 and GM = ISO, the most and least rapidly ventilated GM cases, respectively). Bottom waters in ISO are as young as 23 yr, whereas under GM AABW is at least 400 yr old, substantially older than estimated renewal timescales for this water mass.<sup>2</sup> In addition, the GM terms appear to result in spuriously weak deep ocean currents caused by a flattening of interior density surfaces and thereby a reduction in deep geostrophic flows. This may not be a problem with the GM scheme per se, but more so with our choice of the thickness diffusion parameter  $\kappa$ , which may be more appropriate for the upper Southern Ocean than for deep ocean flows. In addition, downslope plume flows are poorly resolved in  $z$ -level models such as ours, unless some parameterization is made for the bottom boundary layer (see, e.g., Beckmann and Döschner 1997). In any case, the slow downslope flow and weak interior currents under GM explain the spuriously depleted levels of  $^{14}\text{C}$  simulated in CDW.

### c. Indian and Pacific Ocean ventilation

The Indian and Pacific Oceans are ventilated gradually from the south, with more rapid ventilation at the bottom than at middepth (see Figs. 7, 8). The oldest waters of the World Ocean reside in the deep North Pacific (e.g., Broecker et al. 1988), and each model run captures a mid-depth maximum in age in this region (Fig. 9c). Also, all model cases exhibit a gradual aging of bottom water from the Antarctic continent northward. Yet each model case exhibits substantially different ventilation timescales. For example, the oldest NPDW is only 1010 yr in ISO compared to 1340 yr in HOR-Z, 1950 yr in GM-0, and 2010 yr in GM = ISO. Similar age variations are noted in Indian Ocean Deep Water (Table 2).

As stated above, the region of most remote ventilation in all model experiments is the middepth North Pacific Ocean. Figure 15 shows the age of water simulated at the level of oldest North Pacific Deep Water (NPDW) in experiments HOR-Z, ISO, GM = ISO, and GM = 0.5 (runs GM-0 and GM-H are largely similar to GM = ISO). Due to clear differences in the ventilation rate of Antarctic bottom waters (reflected in the age of water south of 60°S in this diagram), the GM and non-GM runs simulate quite different NPDW ages; from under 1000 yr in ISO through to over 1900 yr in GM = ISO. Apart from differing AABW formation rates, the NPDW difference is also due to dramatically weakened interior ocean currents under GM.

The model and observed  $\Delta^{14}\text{C}$  distribution along the GEOSECS Pacific Ocean section is shown in Fig. 16. Waters depleted to  $\Delta^{14}\text{C} < -240\%$  are stippled. The basinwide mean model profiles of  $\Delta^{14}\text{C}$  in the North Pacific Ocean were shown previously in Fig. 10c. A separate radiocarbon diagram was also shown for the Indian Ocean north of the Equator (Fig. 10b). All model experiments simulate a middepth maximum in age and minimum in radiocarbon in the North Pacific near 2500-m depth. However, the simulated ventilation timescales vary greatly between the GM and non-GM runs; typical middepth NPDW is only 900 yr in ISO and 1500–1800 yr in the GM experiments. This is reflected in dramatically different simulations of radiocarbon in NPDW; about  $-180\%$  in ISO and  $-260\%$  to  $-280\%$  in the GM runs (compared with  $-230\%$  to  $-250\%$  in observations). Similar trends can be seen in the Indian Ocean. Overall, the non-GM runs significantly underestimate the ventilation timescales for deep-water renewal in the Pacific and Indian Oceans, whereas the GM runs significantly overestimate these timescales. The GM cases do, however, capture realistic  $^{14}\text{C}$  in the upper 1500 m of the north Indian and Pacific Oceans (Fig. 10).

The timescale for bottom-water ventilation is slowest in the Pacific Ocean in each model run (Table 3). Bottom water in the Pacific can be as old as 770 yr in ISO, compared to 940 in HOR-Z and 1590 in GM-0. Indian Ocean bottom water is renewed over somewhat shorter timescales. The GM runs show consistently older and more  $\Delta^{14}\text{C}$ -depleted bottom water in each ocean basin (see also Figs. 9, 10). This is related to three major changes in ocean circulation and ventilation under GM; namely, substantially reduced formation rates of AABW, the greatly decreased convective activity in the Southern

Ocean, and the weakened deep ocean currents obtained under GM (the latter due to flattened deep isopycnal surfaces).

#### d. Differences between the GM experiments

The radiocarbon and age simulations in the GM experiments are qualitatively quite similar. The most significant changes are realized when the thickness diffusion coefficient  $\kappa$  is halved in GM = 0.5 (see [Figs. 9](#) and [10](#)). Decreasing  $\kappa$  enables more widespread convection, stronger NADW formation, and more rapid deep ocean flows. This results in younger deep waters, particularly in the Atlantic Ocean. The other GM cases (GM-0, GM-H, and GM = ISO) exhibit very similar renewal rates, demonstrating the relative insensitivity of model ventilation to choice of horizontal and/or isopycnal diffusion coefficients. The slightly younger water masses obtained in GM-H compared to GM-0 are due to the weak effects of horizontal diffusion contributing to slightly faster ventilation rates in that run. In GM = ISO, all mixing coefficients are as per run GM-0, only the isopycnal diffusion rate is reduced from the depth-dependent profile used in ISO to a constant value of  $1 \times 10^3 \text{ m}^2 \text{ s}^{-1}$ . As might be expected, this has no significant impact on the interior density structure, resulting in only slightly slower ocean ventilation rates.

### 5. Discussion and conclusions

The sensitivity of interior ventilation timescales to internal ocean mixing schemes has been examined in a global ocean model. We used an idealized “age” tracer that represents the volume-weighted time taken for surface waters to arrive at a given point in the ocean interior. The tracer ages naturally during the model integration, with water that is directly exposed to the sea surface having zero age, and water in the ocean interior aging by the model time step over any given time step. The processes of advection, diffusion, and vertical convection communicate the zero age signal at the sea surface into the ocean interior, limiting the indefinite growth of the age tracer by mixing young waters into the ocean. The resulting age simulations provide a clear diagnosis of model ventilation pathways and timescales. In addition, radiocarbon simulations were conducted to provide a means of comparing the model overturning timescales with those of the real ocean.

#### a. Model case intercomparison

Simulated ventilation timescales and  $^{14}\text{C}$  were found to vary greatly between the HOR, ISO, and GM cases. The isopycnal mixing run exhibits the most rapid water mass renewal due to strong diffusion effects and excessive surface convective overturn, particularly in the Southern Ocean. In contrast, the GM cases show sluggish renewal of deep and bottom waters, with limited vertical convection of surface waters and slower abyssal currents. This overall result of older interior water under GM is consistent with the findings of [Duffy et al. \(1997\)](#) in a mixing sensitivity study of modelled  $\Delta^{14}\text{C}$ . We further find that a background horizontal mixing term or altered isopycnal diffusion do not significantly change interior ocean ventilation rates under GM. This means modelers can adjust these background mixing parameters to minimize numerical problems under GM without dramatically changing their model results. Reducing the GM isopycnal thickness diffusivity, on the other hand, noticeably accelerates the simulated deep-water ventilation rates (largely through increased NADW overturn and more extensive surface layer convection).

In comparison with the HOR runs, deep and bottom water ventilation timescales are reduced by about 30% in ISO, and increased by 30%–40% in the GM cases. This is also reflected in the radiocarbon simulations (see, e.g., [Table 4](#) and [Fig. 10](#)). The GM runs are the least successful in the North Atlantic Ocean, exhibiting very gradual and only shallow water mass renewal compared to observations. This was linked with shallow NADW overturn, limited surface water convection, and slower deep boundary currents. In the Pacific and Indian Oceans, the HOR and ISO runs are ventilated too rapidly due to strong convection and water-mass contribution from the Southern Ocean. In contrast, the GM runs have spuriously old and  $^{14}\text{C}$ -depleted bottom and middepth water. The GM cases do, however, capture realistic  $^{14}\text{C}$  in the upper 1500 m of the Indian and North Pacific Oceans. Overall, none of the model cases we considered could reproduce global ocean ventilation rates over centennial timescales.

#### b. The indirect effects of mixing

A detailed tracer budget analysis over key oceanic regions (not shown) confirms that many of the differences between the simulated age distributions result from differences in the advective velocities and convection patterns in each model run, rather than the mixing terms themselves. That is, the *direct* effects of mixing on the passive age and  $^{14}\text{C}$  tracers are often weaker than the *indirect* effects of changed surface convective overturn and interior ocean currents. The best demonstration of this point is made by comparing experiments ISO and GM-H. The ISO case was seen to have spuriously *young*  $^{14}\text{C}$ -enriched CDW due to excessive Southern Ocean convection and strong AABW formation. The GM-H case had exactly the same mixing parameters as ISO, only GM mixing was included with  $\kappa = 1.0 \times 10^3 \text{ m}^2 \text{ s}^{-1}$ . Yet the GM-H run was found to have spuriously *old* and  $^{14}\text{C}$ -depleted CDW in spite of carrying all the horizontal and isopycnal mixing terms of ISO. This is

due to the absence of deep convective overturn at 55°–70°S and markedly weaker AABW formation under GM, rather than the *direct* effects of GM mixing on the age tracer. In fact, the actual GM thickness diffusion terms act to ventilate or contribute younger waters in the upper 1500 m at 55°–70°S, not age them. Therefore, the GM mixing terms cannot directly account for the older subsurface waters, only indirectly through their influence on interior currents, density, and surface convective overturn. This finding has important implications for choice of model mixing scheme in ocean climate studies.

### c. Comparison with $^{14}\text{C}$ estimates of age

It is of interest to further compare the simulations of seawater age with observed estimates. The distribution of radiocarbon provides the best estimate of deep ocean ventilation rates over long timescales (Stuiver et al. 1983; Broecker et al. 1988). We have already compared modeled and observed radiocarbon directly and therefore would hope to draw consistent conclusions from a comparison of modeled and  $^{14}\text{C}$ -estimated age. A map of the radiocarbon estimated age of water at 3000-m depth is shown in Fig. 17a (redrafted from Broecker et al. 1988). The map was derived by considering the difference between the  $^{14}\text{C}/^{12}\text{C}$  ratio for water at 3000-m depth with that of the overlying surface water, taking into account the natural radioactive decay of  $^{14}\text{C}$  isotopes. The reference  $^{14}\text{C}/^{12}\text{C}$  ratio is therefore somewhat arbitrary, and considering that deep water is formed predominantly in the North Atlantic and Southern Oceans, somewhat inappropriate in certain locations (e.g., the North Pacific). In addition, the estimated age is sensitive to this choice of reference  $^{14}\text{C}/^{12}\text{C}$ , so the error margin on the observed radiocarbon age is rather large. Nevertheless, there is general agreement as to the qualitative trend in age shown in the Broecker et al. (1988) figure. For direct comparison with the model simulations, age at 3000-m depth (interpolated from adjacent model levels) is included for cases HOR-Z, ISO, and GM-0 in Fig. 17. The other GM runs have similar age values to GM-0; GM = ISO having slightly older waters, and GM-H, GM = 0.5 slightly younger waters (refer, e.g., to Fig. 9).


The simulated age of water at 3000-m depth is in reasonable agreement with observed estimates in the North Atlantic Ocean in HOR-Z and ISO, whereas in GM-0 NADW outflow is too confined to the north. This is because the thermohaline overturning is too shallow under GM, with waters of Southern Ocean origin ventilating the deep North Atlantic. Adjacent to Antarctica, young waters appear in approximately the correct location in HOR-Z, whereas they are too diffuse in ISO and too confined to the immediate shelf under GM. It appears that the downslope flow of AABW is far too sluggish in the GM runs, particularly in the Ross Sea. Farther to the north, deep-water age appears quite close to the Broecker et al. (1988) estimates in the Pacific and Indian Oceans under GM, whereas it is too young in ISO and HOR-Z. For example, Indian Ocean Deep Water is estimated to be around 1000–1250 years old in the GM cases and the  $^{14}\text{C}$  estimates, whereas it is only 200–400 yr in ISO and 300–600 yr in HOR-Z. Overall, it appears that each model case has its own problems in reproducing global ocean ventilation timescales within reasonable levels of accuracy.

Since observed radiocarbon is often used as a proxy for water-mass age, it is interesting to compare our simulations of  $^{14}\text{C}$  with the model age tracer. Free from any water mass mixing, oceanic  $\Delta^{14}\text{C}$  would simply equal  $(\Delta^{14}\text{C})_0 \exp(-A/\lambda)$ , where  $A$  is the water mass age in years,  $\lambda$  the decay constant for  $^{14}\text{C}$  (8267 yr), and  $(\Delta^{14}\text{C})_0$  the initial radiocarbon content of the surface source waters. Figure 18 shows scatterplots of simulated  $\Delta^{14}\text{C}$  versus model age in different regions of the ocean in the GM-0 experiment. On the whole, a clear exponential  $^{14}\text{C}$  decay can be seen in the water masses as they age. The spread of  $(\Delta^{14}\text{C})_0$  values in the surface mixed layer (where  $A = 0$ ) is due to  $\Delta^{14}\text{C}$  undersaturation when surface waters are convected downward or when sea ice is present; hence the high spread in surface radiocarbon content in the Southern Ocean. In younger waters, advection processes dominate, so the exponential decay relationship between  $\Delta^{14}\text{C}$  and age is clearly apparent though an offset in  $(\Delta^{14}\text{C})_0$  values gives rise to a stepwise structure in the scatter diagrams. At locations more remote from the direct effects of advection (i.e., in the higher age range), mixing processes become important and so the  $\Delta^{14}\text{C}$ -age relationship is more complex. Also, the nonuniqueness of  $\Delta^{14}\text{C}$  for old water ( $A \approx 1000$  yr) in the Atlantic, Indian, and Pacific Oceans is due to Southern Ocean source waters contributing a spread of  $(\Delta^{14}\text{C})_0$ -age characteristics from the south. In summary, care needs to be taken in extrapolating age values from  $\Delta^{14}\text{C}$  distributions when mixing processes are important or when the  $\Delta^{14}\text{C}$  content of the surface source waters is not well known.

### d. Volumetric age-temperature analyses

The age distributions simulated in the global ocean model can be analyzed in terms of the total volume of ocean occupied by water of a given age. It is useful to map this as a function of potential temperature as well to further distinguish water masses according to location in the ocean. Figure 19 shows a volumetric census of water in the World Ocean as a function of age and potential temperature for the HOR-Z, ISO, and GM-0 cases. The corresponding maps for the other GM cases are similar to GM-0 and so are not included here. Note that a different age scale is adopted for the GM-0 plot. The


majority of water in the model ocean (like the real ocean) has temperature in the 0°–4°C range, so most of the age–temperature census falls into this domain. Water masses drawn along the y axis represent water in the upper mixed layer (having near-zero age), whereas water to the right of the diagram denotes the oldest variety of water of any given temperature.


In each experiment there are typically two relative maxima in the volumetric analysis: one covering the bulk of water in the deep Atlantic, Indian, and Southern Oceans and the other accounting for water in the deep Pacific. For example, NPDW is around 900–1300 yr old in HOR-Z, 600–1000 yr in ISO, and 1300–1900 yr in GM-0. This results in a relatively large volume of water of this age in the 1°–3°C range, clearly evident in [Fig. 19](#) . The Atlantic–Indian–Southern Ocean maxima are typically spread over a greater age range and even appear as two distinct maxima under GM. The two maxima separate the GM Indian Ocean Deep Water (1000–1200 yr) from the GM Atlantic water (700–1000 yr). Under HOR and ISO, with much stronger rates of diapycnal mixing, the age values are more strongly blended across adjacent water masses.

The effects of Southern Ocean convection can be seen in the volumetric age analysis in ISO and HOR-Z, with a large volume of water of near-zero age directly connected to the Atlantic–Indian–Southern Ocean maximum in these two runs. This reflects the direct overturn of surface water over the bulk of the Southern Ocean under ISO and HOR. This is not the case under GM; wherein the main interior water masses are ventilated quite gradually by rather narrow and confined downslope flows. On the volumetric plot, this is reflected in a relatively small volume of young water in the 0°–4°C range in GM-0.


#### *e. Comparison with similar studies using CFCs*

Our Southern Ocean ventilation results under GM appear at first to be in conflict with the findings of similar mixing sensitivity studies (e.g., [England 1995a](#); [Robitaille and Weaver 1995](#); EH97). These studies find a marked improvement in the GM representation of Southern Ocean chlorofluorocarbon (CFC) content compared with standard HOR cases, with substantially reduced convective overturn in subpolar waters and more realistic upper-ocean stratification and vertical CFC gradient. However, CFCs are only decadal timescale transient tracers, whereas natural <sup>14</sup>C resolves long timescale ocean ventilation. As such, analyzing radiocarbon uptake can reveal deficiencies in model circulation that are not necessarily evident using CFCs alone (see review by [England and Maier-Reimer 1999](#)). For example, as in observations, CDW is free of CFCs under GM, whereas it is CFC-laden under ISO and HOR. This represents a model improvement using the GM scheme.

However, the long timescale ventilation of CDW is not accurately represented under GM, as reflected in overly depleted <sup>14</sup>C in that water mass in our study. A key reason for this poor representation of CDW age turns out to be the slow rate of downslope ventilation of AABW under GM (see also [Fig. 14](#) ). This is likely to be because downslope plume flows are poorly resolved in z-level models such as ours, unless some parameterization is made for the bottom boundary layer (see, e.g., [Beckmann and Döscher 1997](#)). Ironically, this problem of sluggish downslope flow rates can be demonstrated by comparing model and observed levels of CFC in recently formed AABW.

[Figure 20](#)  shows a depth profile of the maximum observed signature of CFC-11 in Antarctic waters along the Ajax section of [Warner and Weiss \(1992\)](#). Included for comparison is the corresponding Ajax profile of maximum CFC-11 concentration in our experiments HOR-Z, ISO, and GM-0. Clearly apparent is the overly rapid AABW overturn and spuriously deep open ocean convection of young CFC-laden waters under ISO and HOR ( $\approx 1$  pmol/kg at depth, instead of 0.1–0.2 pmol/kg as observed). This is somewhat corrected under GM, with quite realistic CFC content in the upper 1500 m. However, deeper in the water column, CFC signatures are very weak ( $\approx 0.02$ – $0.03$  pmol/kg) and indeed erroneously underestimated under GM. This is because AABW ventilation rates and downslope flows are too sluggish under this mixing scheme. This is consistent with our findings using  $\Delta^{14}\text{C}$ . Apparently, dense water plumes do not get advected down the Antarctic shelf rapidly enough under GM. Further studies are recommended in this area, particularly with regard to the mechanisms of downslope flow and their sensitivity to the choice of model mixing scheme and vertical coordinate system.

#### *f. Circulation scheme overview*

As an overview of the simulated circulation, ventilation timescales and radiocarbon in each model experiment, [Fig. 21](#)  includes a schematic representation of the major water mass renewal processes in the HOR/ISO and GM cases,

respectively. For comparison, a schematic diagram is also shown of the observed meridional circulation and natural  $\Delta^{14}\text{C}$  distribution in the global ocean. In the diagram, Southern Ocean ventilation is indicated in the Pacific Ocean panels. Overly rapid ventilation of the interior takes place in the Southern Ocean in both HOR and ISO owing to widespread convective overturn, strong AABW production, and in the case of ISO, along-isopycnal mixing in a region of steeply sloping density surfaces. The density surfaces are spuriously steep here because of weak vertical stratification, a result of overly mixed deep waters. These combined processes yield CDW that is too young, too enriched in  $\Delta^{14}\text{C}$ , and insufficiently dense. In contrast, under GM, AABW production is weaker and confined to only a few model grid points, isopycnal surfaces become flatter, and convection is all but shut down in the subpolar waters, yielding much older, denser, and <sup>14</sup>C-depleted CDW.



In the deep Atlantic too much water of Southern Ocean origin ventilates the north in all model experiments, yielding erroneously old and  $^{14}\text{C}$ -depleted water in place of Lower NADW. NADW outflow is confined to the upper 2500 m in ISO and HOR and only the upper 1600-m under GM. In addition, flattened isopycnal surfaces in the GM runs reduce the strength of interior geostrophic flows as compared to ISO and HOR. This acts to reduce the speed of flow in the deep western boundary current in an already viscous model with sluggish deep currents. Halving the GM isopycnal thickness diffusion parameter  $\kappa$  does improve this situation to some degree. A spatially varying parameterization for  $\kappa$  such as that advocated by [Visbeck et al. \(1997\)](#)—one that depends on vertical and horizontal stratification—might yield substantially different baroclinic currents in the region. Our results are consistent with the idea that a value of  $\kappa = 1.0 \times 10^3 \text{ m}^2 \text{ s}^{-1}$  may be reasonable for the upper Southern Ocean, but too high for other regions such as in deep waters and at NADW formation sites. Additional experiments with a spatially varying GM isopycnal thickness diffusion coefficient are recommended.

### *g. Conclusions*

In conclusion, none of the model cases we consider reproduce global ocean ventilation rates over centennial timescales. Overall, the GM runs appear to be reasonably successful in the upper Southern Ocean, particularly with regard to capturing some subpolar density stratification and an older circumpolar water mass in the upper 1500 m. However, GM does not obtain the correct Southern Ocean ventilation timescales and  $\Delta^{14}\text{C}$  content in deep and bottom waters. This appears to be largely due to sluggish bottom boundary flows and weak interior geostrophic currents. In addition, GM is the least successful in the North Atlantic owing to shallow and sluggish NADW outflow. GM does, however, reduce the component of spurious upwelling in the Gulf Stream that is typical of non-GM runs. The ISO and HOR runs behave poorly on account of excessive convection and mixing, most notably in the Southern Ocean.

Modelers have achieved some success with GM in the North Atlantic in simulations run at moderately higher horizontal resolution (e.g.,  $1^\circ \times 1^\circ$ , [Böning et al. 1995](#);  $1.6^\circ \times 2.8^\circ$ , [Hirst and McDougall 1996](#)), although ventilation timescales and radiocarbon were not assessed in those studies. Our model is integrated at the typical resolution of many present-day climate models (approximately  $4^\circ$  in latitude and longitude). GM may require somewhat higher horizontal resolution and a spatially varying thickness diffusion coefficient before it can capture long timescale ocean renewal processes with some degree of fidelity. Even then, it is likely that such a model will require some parameterization of the bottom boundary layer to resolve downslope plume flows in  $z$ -level models. Further studies in this area of research are strongly recommended.

### *Acknowledgments*

The model computations were carried out on the University of New South Wales Cray YMP-EL and the CSIRO Cray YMP 4E/369. MHE acknowledges support from the Australian Research Council. SR acknowledges support from the European Union's Environment and Climate Program. A. C. Hirst kindly provided model code to implement the [Gent and McWilliams \(1990\)](#) mixing scheme. H. Van Den Budenmeyer contributed with discussions on aspects of this work. The detailed comments of two anonymous reviewers greatly helped improve the original manuscript.

---

## REFERENCES

- Beckmann, A., and R. Döscher, 1997: A method for improved representation of dense water spreading over topography in geopotential-coordinate models. *J. Phys. Oceanogr.*, **27**, 581–591.. [Find this article online](#)
- Böning, C. W., W. R. Holland, F. O. Bryan, G. Danabasoglu, and J. C. McWilliams, 1995: An overlooked problem in model simulations of the thermohaline circulation and heat transport in the Atlantic Ocean. *J. Climate*, **8**, 515–523.. [Find this article online](#)
- Broecker, W. S., M. Andree, G. Bonani, W. Woelfli, H. Oeschger, M. Klas, A. Mix, and W. Curry, 1988: Preliminary estimates for the radiocarbon age of deep water in the glacial ocean. *Paleoceanog.*, **3**, 659–699..
- Bryan, K., 1969: A numerical method for the study of the circulation of the world ocean. *J. Comput. Phys.*, **3**, 347–376..
- , and L. J. Lewis, 1979: A water mass model of the world ocean. *J. Geophys. Res.*, **84**, 2503–2517..
- Cox, M. D., 1984: A primitive equation, three-dimensional model of the ocean. GFDL Ocean Group Tech. Rep. No. 1, 143 pp..
- , 1987: Isopycnal diffusion in a  $z$ -coordinate ocean model. *Ocean Modelling* (Unpublished manuscripts) **74**, 1–5..
- Danabasoglu, G., J. C. McWilliams, and P. R. Gent, 1994: The role of mesoscale tracer transports in the global ocean circulation. *Science*, **264**, 1123–1126..

Dixon, K. W., J. L. Bullister, R. H. Gammon, and R. J. Stouffer, 1996: Examining a coupled climate model using CFC-11 as an ocean tracer. *Geophys. Res. Lett.*, **23**, 1957–1960..

Döös, K., and D. J. Webb, 1994: The Deacon cell and other meridional cells of the Southern Ocean. *J. Phys. Oceanogr.*, **24**, 429–442.. [Find this article online](#)

Duffy, P. B., P. Eltgroth, and A. J. Bourgeois, 1995: Improved representation of vertical profiles of temperature and bomb radiocarbon in the GFDL ocean general circulation model. *Geophys. Res. Lett.*, **22**, 1065–1068..

—, K. Caldeira, J. P. Selvaggi, and M. I. Hoffert, 1997: Effect of subgrid-scale mixing parameterizations on simulated distributions of natural  $^{14}\text{C}$ , temperature, and salinity in a three-dimensional ocean general circulation model. *J. Phys. Oceanogr.*, **27**, 498–523.. [Find this article online](#)

Dukowicz, J. K., and R. D. Smith, 1997: Stochastic theory of compressible turbulent fluid transport. *Phys. Fluids*, **9**, 3523–3529..

England, M. H., 1993: Representing the global-scale water masses in ocean general circulation models. *J. Phys. Oceanogr.*, **23**, 1523–1552.. [Find this article online](#)

—, 1995a: Using chlorofluorocarbons to assess ocean climate models. *Geophys. Res. Lett.*, **22**, 3051–3054..

—, 1995b: The age of water and ventilation timescales in a global ocean model. *J. Phys. Oceanogr.*, **25**, 2756–2777.. [Find this article online](#)

—, and A. C. Hirst, 1997: Chlorofluorocarbon uptake in a World Ocean model, 2: Sensitivity to surface thermohaline forcing and subsurface mixing parameterization. *J. Geophys. Res.*, **102**, 15 709–15 731..

—, and G. Holloway, 1998: Simulations of CFC content and water-mass age in the Deep North Atlantic. *J. Geophys. Res.*, **103**, 15 885–15 902..

—, and E. Maier-Reimer, 1999: Using chemical tracers to assess ocean climate models. *Rev. Geophys.*, in press..

—, V. C. Garçon, and J.-F. Minster, 1994: Chlorofluorocarbon uptake in a World Ocean model, 1: Sensitivity to the surface gas forcing. *J. Geophys. Res.*, **99**, 25 215–25 233..

Fiadiero, M. E., 1982: Three-dimensional modeling of tracers in the deep Pacific Ocean, 2, Radiocarbon and the circulation. *J. Mar. Res.*, **40**, 537–550..

Gent, P. R., and J. C. McWilliams, 1990: Isopycnal mixing in ocean circulation models. *J. Phys. Oceanogr.*, **20**, 150–155.. [Find this article online](#)

—, J. Willebrand, T. J. McDougall, and J. C. McWilliams, 1995: Parameterizing eddy-induced tracer transports in ocean circulation models. *J. Phys. Oceanogr.*, **25**, 463–474.. [Find this article online](#)

Hellerman, S., and M. Rosenstein, 1983: Normal monthly wind stress over the World Ocean with error estimates. *J. Phys. Oceanogr.*, **13**, 1093–1104.. [Find this article online](#)

Hirst, A. C., and W. Cai, 1994: Sensitivity of a World Ocean GCM to changes in subsurface mixing parameterization. *J. Phys. Oceanogr.*, **24**, 1256–1279.. [Find this article online](#)

—, and T. J. McDougall, 1996: Deep-water properties and surface buoyancy flux as simulated by a  $z$ -coordinate model including eddy-induced advection. *J. Phys. Oceanogr.*, **26**, 1320–1343.. [Find this article online](#)

—, D. Jackett, and T. J. McDougall, 1996: The meridional overturning cells of a World Ocean model in neutral surface coordinates. *J. Phys. Oceanogr.*, **26**, 775–791.. [Find this article online](#)

Holloway, G., 1992: Representing topographic stress for large-scale ocean models. *J. Phys. Oceanogr.*, **22**, 1033–1046.. [Find this article online](#)

Karoly, D. J., P. C. McIntosh, P. Berrisford, T. J. McDougall, and A. C. Hirst, 1997: Similarities of the Deacon cell in the Southern Ocean and Ferrel cells in the atmosphere. *Quart. J. Roy. Meteor. Soc.*, **122**, 519–526..

Killworth, P. D., 1983: Deep convection in the world ocean. *Rev. Geophys. Space Phys.*, **21**, 1–26..

Levitus, S., 1982: *Climatological Atlas of the World Ocean*. NOAA Prof. Paper No. 13, U.S. Dept. of Commerce, 173 pp..

—, T. P. Boyer, and J. Antonov, 1994: *World Ocean Atlas 1994*, Vols. 1–4, NOAA Atlas NESDIS 1–4, National Oceanographic Data

- Luyten, J., J. Pedlosky, and H. Stommel, 1983: The ventilated thermocline. *J. Phys. Oceanogr.*, **13**, 292–309.. [Find this article online](#)
- Manabe, S., R. J. Stouffer, M. J. Spelman, and K. Bryan, 1991: Transient responses of a coupled ocean–atmosphere model to gradual changes of atmospheric carbon dioxide. Part I: Annual mean response. *J. Climate*, **4**, 785–818.. [Find this article online](#)
- McCartney, M. S., 1977: Subantarctic mode water. A voyage of Discovery. *Deep-Sea Res.*, **24**(Suppl.), 103–119..
- McDougall, T. J., A. C. Hirst, M. H. England, and P. C. McIntosh, 1996: Implications of a new eddy parameterisation for ocean models. *Geophys. Res. Lett.*, **23**, 2085–2088..
- Olbers, D., V. Gouretski, G. Seif, and J. Schroeter, 1992: *The Hydrographic Atlas of the Southern Ocean*. Alfred-Wegener-Institute for Polar and Marine Research, 17 pp and 82 plates..
- Pacanowski, R. C., K. W. Dixon, and A. Rosati, 1991: The GFDL Modular Ocean Model users guide version 1.0. GFDL Ocean Group Tech. Rep. 2, 46 pp..
- Rahmstorf, S., 1995: Multiple convection patterns and thermohaline flow in an idealized OGCM. *J. Climate*, **8**, 3028–3039.. [Find this article online](#)
- Redi, M. H., 1982: Oceanic isopycnal mixing by coordinate rotation. *J. Phys. Oceanogr.*, **12**, 1154–1158.. [Find this article online](#)
- Rix, N. H., and J. Willebrand, 1996: Parameterization of mesoscale eddies as inferred from a high resolution circulation model. *J. Phys. Oceanogr.*, **26**, 2281–2285.. [Find this article online](#)
- Robitaille, D. Y., and A. J. Weaver, 1995: Validation of sub-grid scale mixing schemes using CFCs in a global ocean model. *Geophys. Res. Lett.*, **22**, 2917–2920..
- Schlosser, P., J. L. Bullister, and R. Bayer, 1991: Studies of deep water formation and circulation in the Weddell Sea using natural and anthropogenic tracers. *Mar. Chem.*, **35**, 97–122..
- Stuiver, M., P. D. Quay, and H. G. Ostlund, 1983: Abyssal water Carbon-14 distribution and the age of the world oceans. *Science*, **219**, 849–851..
- Thiele, G., and J. L. Sarmiento, 1990: Tracer dating and ocean ventilation. *J. Geophys. Res.*, **95**, 9377–9391..
- Toggweiler, J. R., K. Dixon, and K. Bryan, 1989: Simulations of radiocarbon in a coarse-resolution world ocean model. I: Steady state prebomb distributions. *J. Geophys. Res.*, **94**, 8217–8242..
- Warner, M. J., and R. F. Weiss, 1992: Chlorofluoromethanes in South Atlantic Antarctic Intermediate Water. *Deep-Sea Res.*, **39**, 2053–2075..
- Visbeck, M., J. Marshall, T. Haine, and M. Spall, 1997: On the specification of eddy transfer coefficients in coarse resolution ocean circulation models. *J. Phys. Oceanogr.*, **27**, 381–402.. [Find this article online](#)
- Weaver, A. J., and E. S. Sarachik, 1990: On the importance of vertical resolution in certain ocean general circulation models. *J. Phys. Oceanogr.*, **20**, 600–609.. [Find this article online](#)

## Tables

Table 1. Experimental design adopted for the present study, including integration times required to equilibrate the age tracer. The different ocean states are integrated until equilibration in  $T$ – $S$  without using vertical acceleration techniques. The age simulations are then conducted over several millennia until a steady-state model age is attained (less than 0.5 year aging per century of integration). The seven cases listed are the Cartesian-mixing experiments (HOR-Z and HOR = 0.75), the isopycnal mixing experiment (ISO), and the Gent and McWilliams (1990) experiments (GM-0, GM-H, GM = ISO, and GM = 0.5);  $A_\rho(z)$  refers to a depth-dependent profile for isopycnal diffusion after Manabe et al. [1991;  $A_\rho = 5.0$  (surface) to  $1.0$  (bottom)  $\times 10^3$  m<sup>2</sup>/s], and  $\kappa$  refers to the GM isopycnal thickness diffusivity.

Experiment	Integration time (yr)	Subgrid-scale eddy parameterization
HOR-Z	4750	Horizontal mixing, $A_{\rho 0} = 1.0$ (surface) to $0.5$ (bottom) $\times 10^3$ m <sup>2</sup> s <sup>-1</sup>
HOR = 0.75	4750	Horizontal mixing ( $A_{\rho 0} = 0.75 \times 10^3$ m <sup>2</sup> s <sup>-1</sup> )
ISO	3650	Isopycnal mixing $A_\rho(z)$ , background $A_{\rho 0} = 0.75 \times 10^3$ m <sup>2</sup> s <sup>-1</sup>
GM-0	3650	GM, $\kappa = 1 \times 10^3$ m <sup>2</sup> s <sup>-1</sup> , isopycnal mixing $A_\rho(z)$ and $A_{\rho 0} = 0$
GM-H	3700	As in GM-0, only $A_{\rho 0} = 0.75 \times 10^3$ m <sup>2</sup> s <sup>-1</sup>
GM = ISO	6250	As in GM-0, only $\kappa = 1 \times 10^3$ m <sup>2</sup> s <sup>-1</sup>
GM = 0.5	5000	As in GM-0, only $\kappa = 0.5 \times 10^3$ m <sup>2</sup> s <sup>-1</sup>

Click on thumbnail for full-sized image.

Table 2. Age (yr) of the oldest water mass mixture obtained in certain regions of the global model experiments: Equatorial Thermocline Water (ETW), North Pacific (NPDW) and Indian (IDW) Ocean Deep Water, Lower North Atlantic Deep Water (LNADW), and Circumpolar Deep Water (CDW). The ETW maximum is the oldest water found at model level 3 (approximately 150-m depth) near the equator. The NPDW and IDW maxima are located at middepth (2000–2500 m) in the northern reaches of the Pacific and Indian Oceans (Figs. 7, 8). The LNADW maxima is taken to be the oldest water obtained north of 40°N between 2500-m and 4000-m depth in the Atlantic Ocean; it should be noted this water has a substantial contribution from AABW in the model experiments (see, e.g., Fig. 5). The oldest CDW is selected from the Southern Ocean between 50°–70°S and depth 1000–3000 m. A set of observed age estimates are given where available, taken from the Broecker et al. (1988) radiocarbon derived estimates of seawater age at 3000 m. All age values are quoted to the nearest 10 yr.

Experiment	ETW	NPDW	IDW	LNADW	CDW
HOR-Z	290	1340	690	480	600
HOR = 0.75	300	1300	640	460	620
ISO	120	1010	420	420	330
GM-0	250	1950	1310	1150	1100
GM-H	240	1920	1280	1120	1070
GM = ISO	370	2010	1360	1190	1190
GM = 0.5	190	1720	1210	850	820
Estimated ( <sup>14</sup> C)		1750	1250	450	800

[Click on thumbnail for full-sized image.](#)

Table 3. Age (yr) of the oldest varieties of bottom water found in the Atlantic, Indian, and Pacific Oceans in each of the model experiments. All age values are quoted to the nearest 10 yr.

Experiment	Atlantic	Indian	Pacific
HOR-Z	460	460	940
HOR = 0.75	510	560	950
ISO	420	360	770
GM-0	1190	1240	1590
GM-H	1130	1200	1560
GM = ISO	1230	1250	1650
GM = 0.5	920	1200	1430

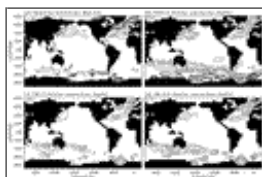
[Click on thumbnail for full-sized image.](#)

Table 4. Mean observed/model values of radiocarbon ( $\Delta^{14}\text{C}$ ) in certain water-mass regions of the global ocean: North Pacific (NPDW) and North Indian (NIDW) Deep Water, Circumpolar Deep Water (CDW), and Lower North Atlantic Deep Water (LNADW). The NPDW and NIDW mean  $\Delta^{14}\text{C}$  are taken in the Pacific/Indian regions north of the Equator between 2000-m and 3000-m depth. The CDW value is the mean Southern Ocean  $\Delta^{14}\text{C}$  at depth 1500–3000 m between 55° and 70°S. The LNADW value is the mean  $\Delta^{14}\text{C}$  at 0°–60°N between 3000 and 4000 m in the Atlantic Ocean; it should be noted this water has a substantial contribution from AABW in the model experiments (see, e.g., Fig. 5). Values are quoted to the nearest ‰.

Experiment	NPDW	NIDW	CDW	LNADW
HOR-Z	-208	-149	-122	-136
HOR = 0.75	-212	-147	-129	-142
ISO	-183	-137	-118	-139
GM-0	-276	-232	-203	-223
GM = ISO	-279	-235	-208	-221
GM = 0.5	-265	-227	-181	-199
Observed	-240	-193	-161	-78

[Click on thumbnail for full-sized image.](#)

## Figures



[Click on thumbnail for full-sized image.](#)

Fig. 1. (a) Winter mixed layer depth (m) calculated from the [Levitus et al. \(1994\)](#) climatology adopting a density change criterion of  $0.125 \text{ kg m}^{-3}$  for the base of the mixed layer. (b)–(d) Maximum convection depth (m) during an annual cycle of the equilibrated ocean states for experiments HOR-Z, GM-0, and GM = 0.5. Contour levels are chosen that coincide with successive model level depths. Regions of convective overturn greater than 120 m are stippled.

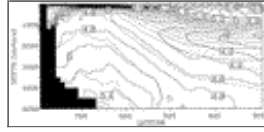






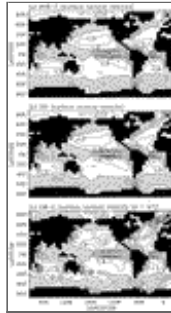
Click on thumbnail for full-sized image.

Fig. 2. Latitude–depth sections of potential density ( $\text{kg m}^{-3}$ ) at  $180^\circ$ : (a) observed, (b) ISO, and (c) GM-0. The  $180^\circ$  section exemplifies the typical slope of density surfaces in the Southern Ocean in both observations and the model runs.



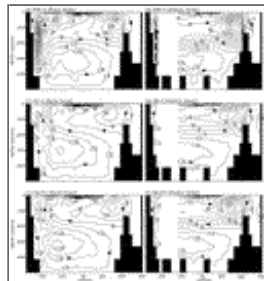
Click on thumbnail for full-sized image.

Fig. 3. Zonal mean concentration of dissolved oxygen in milliliters per liter from the annual mean climatology of [Olbers et al. \(1992\)](#). Concentrations weaker than  $4.4 \text{ ml l}^{-1}$  are shaded. Dashed contours indicate the location of zonal mean neutral surface trajectories. Surfaces are assumed to follow contours of potential density referenced to the surface in the upper 540 m, referenced to 1500 m over the interval 540–2300 m and referenced to 3000 m at depths below 2300 m. Contour interval is  $0.2 \text{ ml l}^{-1}$  for oxygen and nonuniform for neutral surfaces.



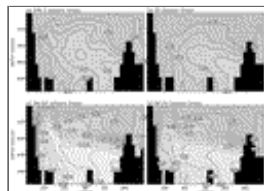
Click on thumbnail for full-sized image.

Fig. 4. Vertical velocity ( $10^{-6} \text{ m s}^{-1}$ ) at 51-m depth for the (a) HOR-Z, (b) ISO, and (c) GM-0 experiments. Included in the GM-0 distribution is the additional vertical tracer advection transport ( $w^*$ ) of [Gent et al. \(1995\)](#). Shaded regions denote surface level upwelling. Contours are drawn at uniform intervals of  $10^{-6} \text{ m s}^{-1}$ .



Click on thumbnail for full-sized image.

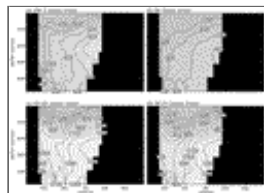
Fig. 5. Annual-mean meridional overturning (Sv) in HOR-Z, GM-0, and GM = 0.5 for the global and Atlantic Oceans. No contours are drawn in the Atlantic sector where the model is free to exchange water zonally. Contour interval is 4 and 2 Sv, respectively, for the global and Atlantic Ocean sections. Meridional overturning values shown for the GM runs include the additional tracer advection transports of [Gent et al. \(1995\)](#). Overturning in the other experiments is not shown since ISO and HOR = 0.75 are very similar to HOR-Z, and GM-H and GM = ISO are largely similar to GM-0.



Click on thumbnail for full-sized image.

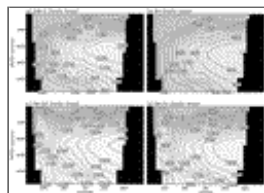
Fig. 6. Basin-averaged age (years) in the Atlantic Ocean for experiments HOR-Z, ISO, GM = ISO, and GM = 0.5. The GM = ISO

and GM = 0.5 cases were selected as they represent the GM runs with the oldest and youngest deep waters, respectively (refer also to [Table 2](#)). The other GM runs (GM-0 and GM-H) are closest to GM = ISO in terms of their simulated age. Contour interval is 100 yr. Stippling density decreases with age.



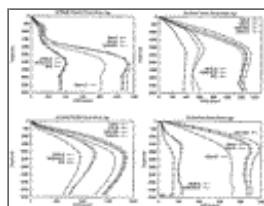
[Click on thumbnail for full-sized image.](#)

Fig. 7. As in [Fig. 6](#) but for the Indian Ocean.



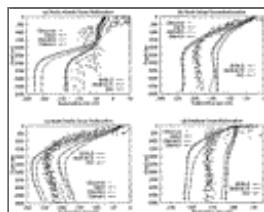
[Click on thumbnail for full-sized image.](#)

Fig. 8. As in [Fig. 6](#) but for the Pacific Ocean.



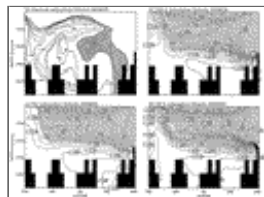
[Click on thumbnail for full-sized image.](#)

Fig. 9. Basinwide mean model profiles of age (years) in (a) the North Atlantic (0°–70°N), (b) the North Indian, (c) the North Pacific (0°–70°N), and (d) the Southern Ocean (55°–70°S). Note the difference in scaling along the age axis in each panel.



[Click on thumbnail for full-sized image.](#)

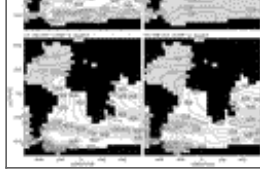
Fig. 10. Basinwide mean model profiles of radiocarbon (‰) in (a) the North Atlantic (0°–70°N), (b) the North Indian, (c) the North Pacific (0°–70°N), and (d) the Southern Ocean (55°–70°S). Corresponding GEOSECS observations of  $\Delta^{14}\text{C}$  are included for comparison.



[Click on thumbnail for full-sized image.](#)

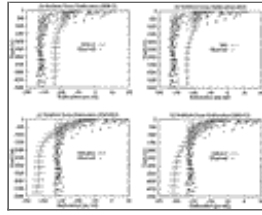
Fig. 11. Observed western Atlantic GEOSECS  $\Delta^{14}\text{C}$  compared with model runs HOR-Z, ISO, and GM-0. Contour interval is -10‰ and stippling indicates waters with  $\Delta^{14}\text{C}$  content greater than -90‰. In the observed section, no contours are drawn in regions contaminated by bomb-produced  $^{14}\text{C}$ .





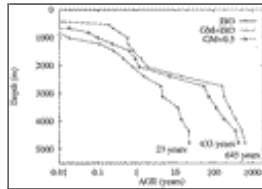
Click on thumbnail for full-sized image.

Fig. 12. Age of water on the level of most rapid NADW outflow for experiments (a) HOR-Z, (b) ISO, (c) GM = ISO, and (d) GM = 0.5. Contour interval is 50 yr. Water younger than 250 yr is stippled.



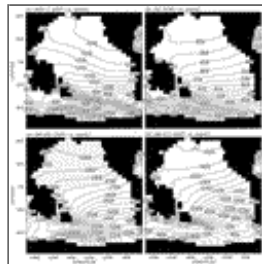
Click on thumbnail for full-sized image.

Fig. 13. Model simulations of radiocarbon at the latitude band  $55^{\circ}$ – $70^{\circ}$ S, shown as a mean profile with standard deviation bars to indicate the spread of  $^{14}\text{C}$  simulated at each depth level. (a) HOR-Z, (b) ISO, (c) GM = ISO, and (d) GM = 0.5. The overlaying scatterplot of GEOSECS  $^{14}\text{C}$  measurements facilitates a direct comparison between modeled and observed ventilation rates. This region corresponds in the real ocean with the location of CDW upwelling and relatively stable surface layer stratification (e.g., Figs. 2a and 3).



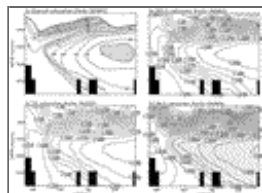
Click on thumbnail for full-sized image.

Fig. 14. Depth profiles of minimum age of AABW in ISO and two of the GM runs (GM = 0.5 and GM = ISO; the most and least rapidly ventilated GM cases, respectively). The age scale is logarithmic. Youngest bottom water ages are given for the deepest model level.



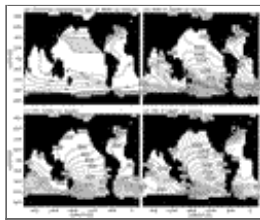
Click on thumbnail for full-sized image.

Fig. 15. Age of water on the level of oldest North Pacific Deep Water for experiments (a) HOR-Z, (b) ISO, (c) GM = ISO, and (d) GM = 0.5. Contour interval is 50 yr. Water younger than 250 yr is densely stippled; water older than 1750 yr is coarsely stippled (for comparison with Fig. 17a).



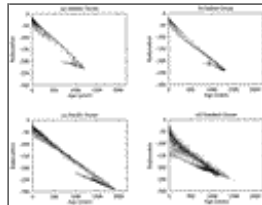
Click on thumbnail for full-sized image.

Fig. 16. Observed Pacific Ocean GEOSECS  $\Delta^{14}\text{C}$  compared with model runs HOR-Z, ISO, and GM-0. Contour interval is  $-1.0\text{‰}$  and stippling indicates waters with  $\Delta^{14}\text{C}$  content less than  $-240\text{‰}$ . In the observed section, no contours are drawn in regions contaminated by bomb-produced  $^{14}\text{C}$ .



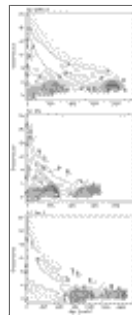
Click on thumbnail for full-sized image.

Fig. 17. (a) Radiocarbon derived estimates of water age (years) at 3000-m depth in the global ocean as estimated by [Broecker et al. \(1988\)](#) referencing  $^{14}\text{C}/^{12}\text{C}$  ratios at 3-km depth relative to those of the overlying surface water. Contour interval is 250 yr with additional contours drawn in the North Atlantic. (b)–(d) Age of water at 3000-m depth in three model experiments (HOR-Z, ISO, and GM-0). Values are obtained by interpolating from the two adjacent model levels near 3000 m. Contour interval is 50 yr. Water younger than 250 yr is densely stippled; water older than 1750 yr is coarsely stippled.



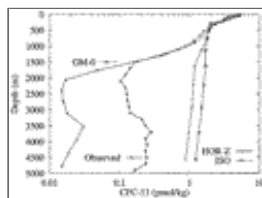
Click on thumbnail for full-sized image.

Fig. 18. Scatter diagrams of simulated  $\Delta^{14}\text{C}$  vs model age in different regions of the ocean in the GM-0 experiment. (a) The Atlantic Ocean (40°S–75°N), (b) the Indian Ocean (north of 40°S), (c) the Pacific Ocean (40°S–65°N), and (d) the Southern Ocean (south of 40°S).



Click on thumbnail for full-sized image.

Fig. 19. Volumetric age–potential temperature analysis for the (a) HOR-Z, (b) ISO, and (c) GM-0 experiments. The other GM cases are similar to GM-0, particularly GM-H and GM = ISO. The volumetric census is performed by binning water masses over a uniform mesh with  $1^\circ\text{C}$  and 30-yr incrementation. Contours are drawn every  $10^6 \text{ km}^3$ . Light stippling indicates a total volume of less than  $10^6 \text{ km}^3$ , whereas dense stippling indicates an integrated volume in excess of  $5 \times 10^6 \text{ km}^3$ . Note the difference in scaling along the age axis of the GM-0 panel.

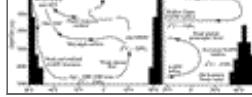


Click on thumbnail for full-sized image.

Fig. 20. Observed and modeled depth profile of the maximum signature of CFC-11 in Antarctic waters along the Ajax section of [Warner and Weiss \(1992\)](#). A logarithmic scale for CFC-11 is used to highlight differences in the bottom water signature of the transient CFC tracer.







[Click on thumbnail for full-sized image.](#)

Fig. 21. Schematic overview of the large-scale water mass renewal processes and  $\Delta^{14}\text{C}$ -age distributions (a) observed, (b) in the HOR and ISO experiments, and (c) in the GM runs. Only the Southern, Pacific, and Atlantic Oceans are shown. The Indian Ocean behaves in a similar way to the Pacific, only with a reduced northern extent.

<sup>1</sup> [England and Holloway \(1998\)](#) find improved CFC burdens in Upper NADW when adopting the topographic stress parameterization of [Holloway \(1992\)](#) in a HOR simulation.

<sup>2</sup> [Schlosser et al. \(1991\)](#) estimate an upper bound of 14 yr for pure Weddell Sea Bottom Water on the basis of CFC-11/CFC-12 observations.

\* Additional affiliation: CSIRO/Atmospheric Research, Aspendale, Victoria, Australia.

*Corresponding author address:* Dr. Matthew England, Centre for Environmental Modelling and Prediction (CEMAP), School of Mathematics, University of New South Wales, NSW 2052, Australia.

E-mail: [M.England@unsw.edu.au](mailto:M.England@unsw.edu.au)

[top ▲](#)



© 2008 American Meteorological Society [Privacy Policy and Disclaimer](#)  
Headquarters: 45 Beacon Street Boston, MA 02108-3693  
DC Office: 1120 G Street, NW, Suite 800 Washington DC, 20005-3826  
[amsinfo@ametsoc.org](mailto:amsinfo@ametsoc.org) Phone: 617-227-2425 Fax: 617-742-8718  
[Allen Press, Inc.](#) assists in the online publication of *AMS* journals.